# Parallel in-plane-gated wires coupled by a ballistic window

Y. Hirayama,* A. D. Wieck,* T. Bever, K. von Klitzing, and K. Ploog†
*Max-Planck-Institut für Festkörperforschung, Heisenbergstrasse 1, D-7000 Stuttgart 80, Germany*
(Received 28 January 1992; revised manuscript received 7 April 1992)

Two parallel in-plane-gated (IPG) wires are coupled by a ballistic window. The ballistic window is rectangular, and the four terminals have a different arrangement from the usual fourfold-symmetry structures (such as a wire cross) where alternate terminals face each other. The ballistic coupling is achieved between two parallel wires by a sideways component but not by a straightforward component, and the four-terminal resistance (or transfer resistance) becomes negative at zero magnetic field. The amount of a sideways ballistic component is sensitive to a subband depopulation in each wire. The modulation of a sideways ballistic component results in a distinct oscillation in the four-terminal resistance as a function of the IPG voltage. The magneto-depopulation of one-dimensional subbands in each wire is also clearly observed in this system.

## I. INTRODUCTION

Since the experimental observation of quantized conductance,[1] many interesting experimental and theoretical studies have been reported for ballistic low-dimensional systems.[2] In particular, when a number of constrictions are placed within the electron mean free path, the coupling of ballistic trajectories lead to exciting phenomena,[3–8] such as large magneto-depopulation and interference effects in parallel ballistic point contacts[5] and commensurate orbits in antidot systems.[6] In a small ballistic structure with four terminals, Ford *et al.*[7] observed many resonant features in the four-terminal resistance. Furthermore, Smith *et al.*[8] performed Fabry-Pérot interferometry with electron waves by modulating the cavity length using depletion-edge-position control. On the other hand, a coupling of parallel wires is expected to make a functional system analogous to microwave or optical waveguides.[9] Electron wave interference may occur by wave coupling through a narrow barrier or through a number of openings. However, coupling characteristics between two wires are not yet clear even for a fundamental structure where two wires are coupled by a single window.

In this paper we discuss transport characteristics of parallel wires coupled by a ballistic window (see Fig. 1). The long (5-$\mu$m) in-plane gates (IPG's) definitely confine each terminal to the wire structure and an effective wire width is modulated by applying a voltage to the in-plane gates. This structure is also considered a ballistic four-terminal or transfer-resistance configuration,[10] where both current and voltage probes exist within the ballistic mean free path. The four-terminal resistance of such a structure is very sensitive to the electron wave motion inside the ballistic region. In particular, the subband effects of each terminal wire produce interesting phenomena.

## II. RESULTS AND DISCUSSION

The carrier density ($n$) and mobility ($\mu$) of the nonilluminated two-dimensional (2D) electron gas in the GaAs/$Al_xGa_{1-x}As$ heterostructure at 1.5 K were $1.6\times10^{11}$ cm$^{-2}$ and $5\times10^{5}$ cm$^2$/V s, respectively. The carrier density was gradually increased by repeating a brief illumination at 1.5 K. The confined electron-gas system shown in Fig. 1 was formed by focused Ga ion-beam [Ga focused-ion-beam (FIB)] scanning.[11] The beam diameter was about 100 nm and the ion dose was about $10^{12}$ cm$^{-2}$. Subsequent annealing was carried out at 730 °C. Ohmic contacts (Au/Ge/Ni) were formed to each 2D electron-gas region labeled 1–6. Regions 5 and 6 act as IPG's (Refs. 12 and 13) and were used to control the conductivities of two parallel wires by $V_{g5}$ and $V_{g6}$. The conductance characteristics were measured using a lock-in technique with a constant ac current of 5 nA. In our experiments, we set $V_g=V_{g5}=V_{g6}$ to maintain the twofold symmetry of the system.[14] In this paper, we show the data measured at 1.5 K. Interference effects (such as Fabry-Pérot mode) in the ballistic window is suppressed at $T>1$ K because of the large size of the window region (at least $2W\geq1.3$ $\mu$m as shown later). Then, subband effects and classical ballistic effects appear prominently at 1.5 K.

The observed four-terminal (transfer) resistance $R_{L1}=R_{12,34}=(V_3-V_4)/I_{1\text{-}2}$ is shown in Fig. 1(c) as a function of magnetic field. $R_{L1}$ is proportional to $T_{31}T_{42}-T_{32}T_{41}$ according to the Büttiker-Landauer formula,[15] where $T_{ij}$ is the transmission probability from terminals $j$ to $i$. When the window region is ballistic, $T_{32}$ and $T_{41}$ include some trajectories directly from 1 (or 2) to 4 (or 3) without scattering (including boundary reflection) in the window region. We refer to these trajectories as the sideways ballistic component. There are no such trajectories for $T_{31}$ and $T_{42}$. Then, $T_{32}T_{41}>T_{31}T_{42}$ and $R_{L1}<0$ at $B=0$ T. The negative peak of $R_{L1}$ at $B=0$ T in Fig. 1(c) thus clearly indicates the existence of a sideways ballistic component in the system with $W=1.25$ $\mu$m and $L=1.2$ $\mu$m. The four-terminal resistance with cyclically changed contacts $R_{L2}=R_{42,31}=(V_3-V_1)/I_{4\text{-}2}$ and Hall resistance $R_H=R_{32,41}=(V_4-V_1)/I_{3\text{-}2}$ were also measured for the same sample (but at slightly different carrier densities) and compared in Fig. 2 with $R_{L1}$. The

 

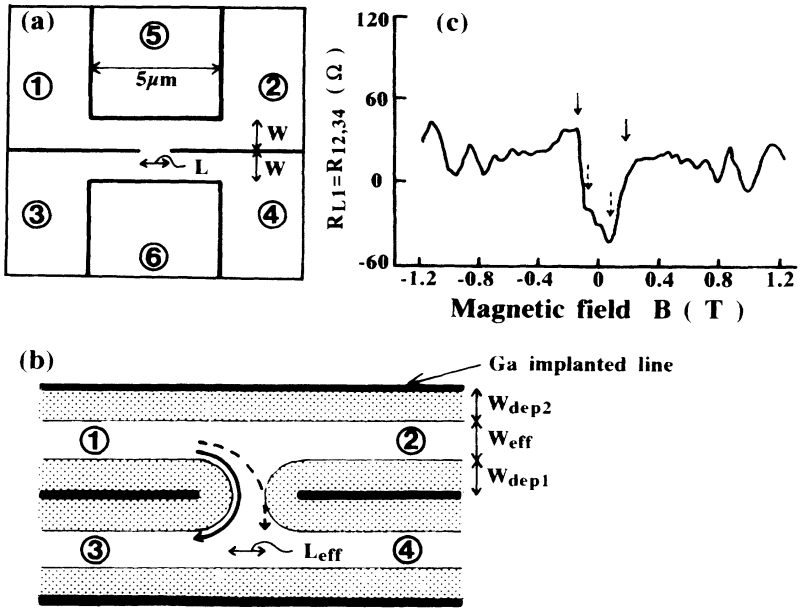


FIG. 1. (a) Schematic diagram of two parallel IPG wires coupled by a ballistic window. The focused Ga ion beam was scanned along the solid lines. (b) Magnified diagram around the window region. Dotted area represents the depletion region spreading. (c) Typical $R_{L1}=R_{12,34}$ vs magnetic-field characteristics of the structure with $W=1.25$ μm, $L=1.2$ μm, and $V_g=0$ V measured in a low magnetic field. The 2D carrier density is $1.8\times10^{11}$ cm$^{-2}$. Solid arrows indicate the magnetic field ($B=B_{c1}$) where the negative peak disappears and broken arrows indicate the magnetic field ($B=B_{c2}$) where a second peak or a kink appears in the negative peak.

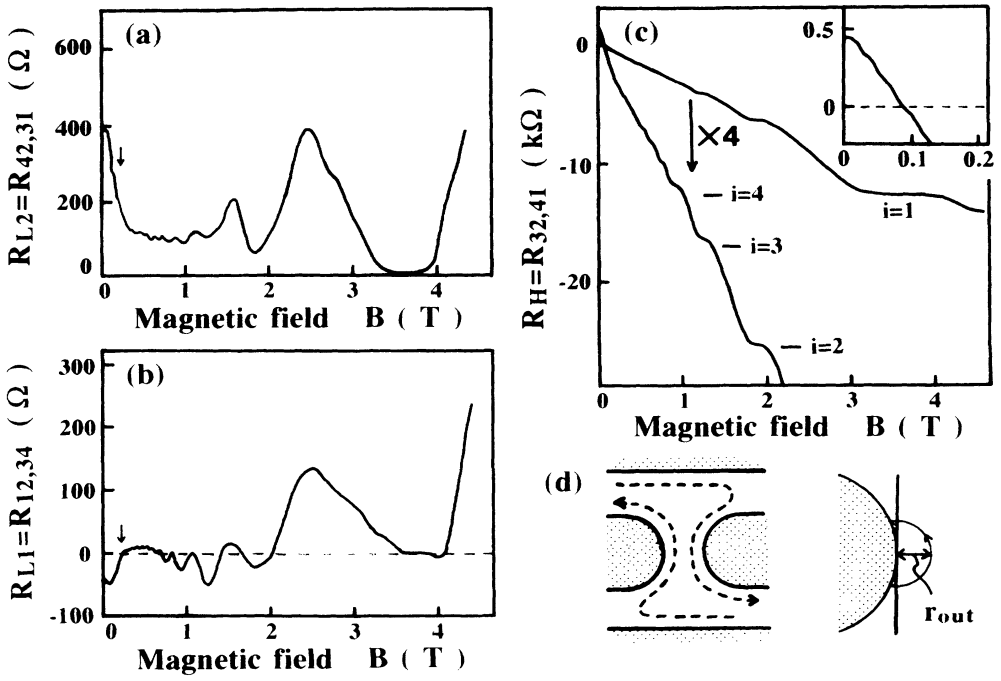


FIG. 2. (a) $R_{L2}=R_{42,31}$, (b) $R_{L1}=R_{12,34}$, and (c) $R_H=R_{32,41}$ obtained for the sample of Fig. 1 at $T=1.5$ K. The carrier density is $2\times10^{11}$ cm$^{-2}$ and $V_g=0$ V. Solid arrows indicate the approximate position of $B_{c1}$. The inset of (c) shows a magnification near $B=0$ T with the same axis labeling as the main figure. (d) A possible trajectory for the combination of straight and rounded boundaries (left) and the change in the area enclosed by a trajectory for straight and rounded boundaries with the same $r_{out}$ (right).

Hall resistance ($R_H$) shows the quantized plateaus ($h/2e^2i$, where $i$ denotes the integer) in the high magnetic region. The SdH oscillations are observed in both $R_{L1}$ and $R_{L2}$. The index and $B^{-1}$ plot of resistance minima falls on a straight line. The slope of this line and the average slope of $R_H$ give the carrier density $n$ of $2\times10^{11}$ $cm^{-2}$ in the window region.

In a normal wire cross, a ballistic coupling is achieved between two wires facing each other. Then, both $T_{32}$ and $T_{41}$ decrease with magnetic field. In this case, a negative "bend resistance" smoothly disappears as a function of magnetic field.[16] However, a ballistic coupling is achieved between staggered wires by a sideways component in the present system. A direct transmission probability from 1 to 4 is probably more enhanced at $B=B_{c2}$, where a straightforward injection makes a trajectory as shown by the broken line in Fig. 1(b), than at $B=0$ T. This effect may result in a kink or a second peak appearing in the negative peak of $R_{L1}$ [see broken arrows in Fig. 1(c)]. The negative peak disappears at $B=B_{c1}$, where $R_{L2}$ decreases drastically. At this field, almost all trajectories emitted from 1 are absorbed into 3. Although it is difficult to discuss $B_{c1}$ and $B_{c2}$ in detail, they become a function of $W_{\rm depl}$, $W_{\rm eff}$, and $n$. In addition, it is noteworthy that both $B_{c1}$ and $B_{c2}$ are determined by $W_{\rm depl}$ and $n$ when $W_{\rm eff}$ is small.

Another interesting feature in Fig. 2 is the behavior of $R_{L1}$ as a function of magnetic field. After the disappearance of the negative peak around $B=0$ T, $R_{L1}$ becomes almost zero. This is because $T_{31}T_{42}\approx T_{32}T_{41}$ by a scrambling effect. However, the resistance minima again become negative in an intermediate-field region. This negative region was observed at 1.5 K for several structures with different sizes and carrier densities and also when the magnetic-field direction was reversed. In a high field, the quantum Hall effect appears and the resistance minima in $R_{L1}$ return to zero ($T_{32}T_{42}=T_{32}T_{41}=0$). Furthermore, the negative $R_{L1}$ in an intermediate field becomes weak when $R_{L1}$ is measured at lower temperature ($T\leq100$ mK). These results indicate that this negative $R_{L1}$ relates to an incomplete formation of edge channels. Although the origin of this negative $R_{L1}$ is not yet clear, an explanation may be that our structure consists of both straight and rounded boundaries. When the maximum distance of a skipping trajectory from the boundary ($r_{\rm out}$) becomes smaller, the trajectory is absorbed into the next terminal wire with a higher probability. If $l_{\rm cyc}$ [cyclotron radius $(2mE_F)^{1/2}/eB$] is not much smaller than the diameter of a rounded depletion edge ($\approx W_{\rm depl}$), the skipping trajectory satisfying Bohr-Sommerfeld quantization [$B(\text{area})=h(k-\frac{1}{4})/e, k$:integer] (Ref. 17) has a larger $r_{\rm out}$ for a straight boundary than for a rounded one [see Fig. 2(d)]. This suggests a possibility of trajectories [broken line trajectories in Fig. 2(d)] that are reflected at the end of a straight boundary but absorbed into the next terminal after skipping along a rounded boundary. Such a possibility increases $T_{41}$. When edge channels are completely established, $T_{32}$ becomes zero in spite of the fact that $T_{41}$ increases by the trajectory shown in Fig. 2(d). Then $T_{32}T_{41}=0$ and no negative resistance appears. This may be the case with the lower temperature (mK-order) measurements. However, $T_{32}$ is not zero in a low magnetic-field region at 1.5 K due to an incomplete formation of edge channels. Therefore, we can expect that the increase of $T_{41}$ disturbs the balance between $T_{31}T_{42}$ and $T_{32}T_{41}$ and pushes $R_{L1}$ to negative. With increasing magnetic field, $l_{\rm cyc}\ll W_{\rm depl}$. Then, this effect disappears at $B\geq2$ T. Finally, $T_{42}=T_{32}=T_{41}=0$ and the resistance minima of $R_{L1}$ become zero in a high field. Another possibility is that slight differences in the wire width between the four terminal wires also enhance $T_{41}$ (or $T_{32}$), then produce such negative resistance under the condition of the incomplete edge channels.

The transport characteristics were also measured for systems with narrower effective-width terminal wires. The narrow $W_{\rm eff}$ systems satisfying symmetric characteristics ($R_{12,12}\approx R_{34,34}$) were realized with a carrier density ($n$) of $1.6\times10^{11}$ $cm^{-2}$ (at $V_g=0$ V) for $W=1.25$ $\mu$m and $L=1.2$ $\mu$m structure and $2.3\times10^{11}$ $cm^{-2}$ (at $V_g=0$ V) for $W=0.65$ $\mu$m and $L=0.6$ $\mu$m structure. In these systems, the IPG voltage ($V_g$) was varied and all parameters $R_{L1}$, $R_{L2}$, and $R_H$ were measured as a function of magnetic field for each $V_g$. Here, we show $R_{L1}$ observed in the structure with $W=1.25$ $\mu$m and $L=1.2$ $\mu$m (Fig. 3). Clear negative peaks around $B=0$ T are found for all measurements. It is important that both $B_{c1}$ and $B_{c2}$ are not sensitive to the variation in $V_g$. Therefore, the value of $W_{\rm depl}$ is considered to be almost independent of $V_g$, although a carrier-density variation with $V_g$ might induce a slight change in $W_{\rm depl}$. This also means that $L_{\rm eff}\approx L-2W_{\rm depl}$ is kept at a constant value. The IPG voltage preferentially modulates the depletion-region spreading of the gate side ($W_{\rm dep2}$) and consequently $W_{\rm eff}$, because this voltage is applied between the channel and the gate and intrinsically does not influence the depletion around the FIB lines on the symmetry axis of the structure.

On the other hand, oscillation structures are clearly observed in $R_{L1}$ down to a low magnetic field in Fig. 3 and they are varied as a function of $V_g$. In this configuration, electrons are injected parallel to the boundaries rather than at right angles. Furthermore, the boundaries between terminals 1 and 3 (and 2 and 4) are rounded rather than straight. Therefore, it is difficult to consider the geometrical effects, such as electron focusing. As shown in Fig. 3 (inset), the position of resistance minima correlates well with the SdH oscillation in a high magnetic field. The deviation from the straight line in a fan diagram is observable only when $W_{\rm eff}$ is narrow enough. Thus, we assume that the observed results come from a subband depopulation in each terminal wire.[18] Figure 3 indicates the occupation of about seven subbands at $B=0$ T for $V_g\approx0$ V. This subband number approximately corresponds to $W_{\rm eff}=240$ nm. Thus, we can assume $W_{\rm depl}=W_{\rm dep2}\approx500$ nm at $V_g=0$ V [including half the width of the Ga-implanted line (about 50 nm)]. The depopulation characteristics shown in the inset of Fig. 3 agree with $W_{\rm eff}=200$ nm (about six subbands) and $W_{\rm eff}=400$ nm (12–14 subbands) at $V_g=-0.25$ and 1 V, respectively. The $V_g$-independent $W_{\rm depl}=500$ nm in-

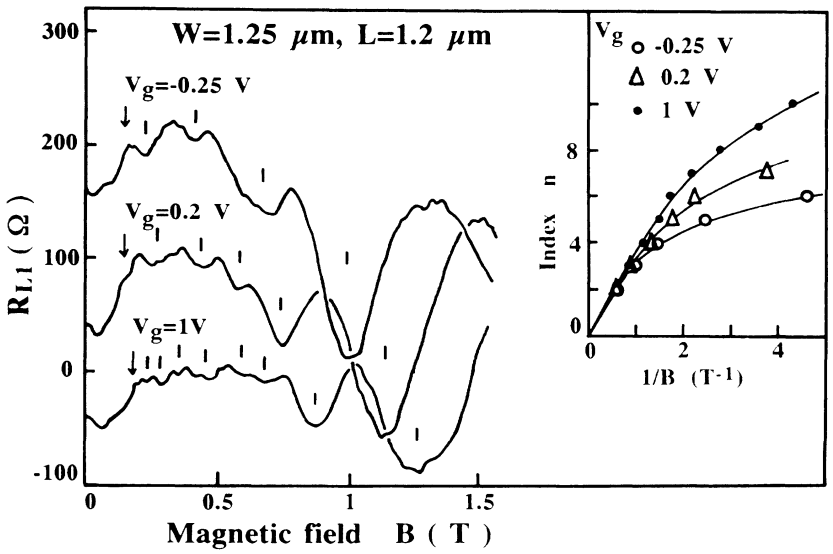


FIG. 3. $R_{L1}$ as a function of magnetic field when the effective width of terminal wires is narrow. Solid arrows indicate the approximate position of $B_{c1}$. Solid bars indicate resistance minima of SdH oscillation originating from subband depopulation of terminal wires. $W=1.25$ μm and $L=1.2$ μm. Carrier density is $(1.5-1.8)\times10^{11}$ cm$^{-2}$ for $V_g=0.25-1$ V. Each curve is offset by 100 Ω for clarity. Fan plots of resistance minima are shown in the inset.

duces $W_{dep2}=550$ nm ($V_g=-0.25$ V) and $W_{dep2}=350$ nm ($V_g=1$ V). This change in $W_{dep2}$ with $V_g$ is reasonable with the estimation of $W_{dep2}$ from the transport characteristics of simple IPG wires with similar carrier density.[13] Although there is an overlap of some small signals in Fig. 3, the depopulation corresponding to $L_{eff}$ is not clear in Fig. 3 in spite of the estimated $L_{eff}$ of 300 nm. The spreading of the depletion region at the edge of Ga-scanned line is difficult to estimate and $L_{eff}$ may be larger than 300 nm. The estimated number of subbands indicates that subband depopulation occurs within an IPG voltage interval of $\Delta V_g=0.17-0.21$ V. For the narrower system ($W=0.65$ μm, $L=0.6$ μm and $n=2.3\times10^{11}$ cm$^{-2}$ at $V_g=0$ V), similar oscillation structures are observed in $R_{L1}$. The depopulation characteristics are obtained in the same manner as shown in Fig. 3 and results indicate that depopulation of the subband in each terminal wire occurs within a $V_g$ interval of $\Delta V_g=0.12-0.16$ V.

Finally, we show $R_{L1}$ (at $B=0$ T) as a function of $V_g$ for several structures in Fig. 4. For (a) $W=0.65$ μm, $L=0.6$ μm and (b) $W=1.25$ μm, $L=1.2$ μm the measurements were carried out at the carrier density described in the previous paragraph. The carrier density of $1.6\times10^{11}$ cm$^{-2}$ ($V_g=0$ V), which was the same carrier density as that in (b), was used for the structure with (c) $W=1.25$ μm and $L=2.7$ μm. For (a) and (b), $R_{L1}$ becomes negative for almost all IPG voltages, and oscillatory structures appear in the $R_{L1}$ vs $V_g$ curve. These oscillations were clearly observed in $R_{L1}$ when two parallel wires indicated good symmetry and the wire width was sufficiently narrow. The subband depopulation intervals of $\Delta V_g=0.12-0.16$ V [for the condition of Fig. 4(a)] and $\Delta V_g=0.17-0.21$ V [for Fig. 4(b)] discussed in the previous paragraph approximately agree with the oscillation period of $R_{L1}$ observed in Fig. 4. Therefore, we conclude that these oscillations originate from 1D subband depopulation of each terminal wire. As discussed before, the direct ballistic component from 1 to 4 (or 2 to 3) induces negative $R_{L1}$. In the semiclassical view, this situation is represented by a trajectory shown in Fig. 4(d). Such a component is enhanced when the Fermi energy lies just above the 1D subband of a terminal wire and a transverse momentum of injected electrons becomes large compared to the straight momentum.[19] With increasing Fermi energy, the straight momentum increases and the sideways ballistic component through the window becomes small. When there is no direct coupling through the ballistic window, the trajectories are equally divided between terminals 3 and 4, and then $R_{L1}$ reaches 0. These oscillations of sideways ballistic components are sensitively detected in $R_{L1}$ and result in the oscillations shown in Fig. 4. Many functional devices have been proposed for ballistic systems based on the analogy with electromagnetic waveguides. Coupling between two parallel waveguides through more than two windows is expected to make an interesting functional operation through wave interference effects. However, the present experiments with a single window indicate that oscillatory structures can be induced not only by the interference effects but also by subband effects when several 1D subbands in the wire are occupied. These results also make a striking contrast with many experiments on metal systems,[20] where the subband separation is so small that subband effects are negligible.

For a longer window structure [$L=2.7$ μm, Fig. 4(c)], $R_{L1}$ becomes positive. In this case the system is no longer completely ballistic and $R_{L1}$ includes a diffusive

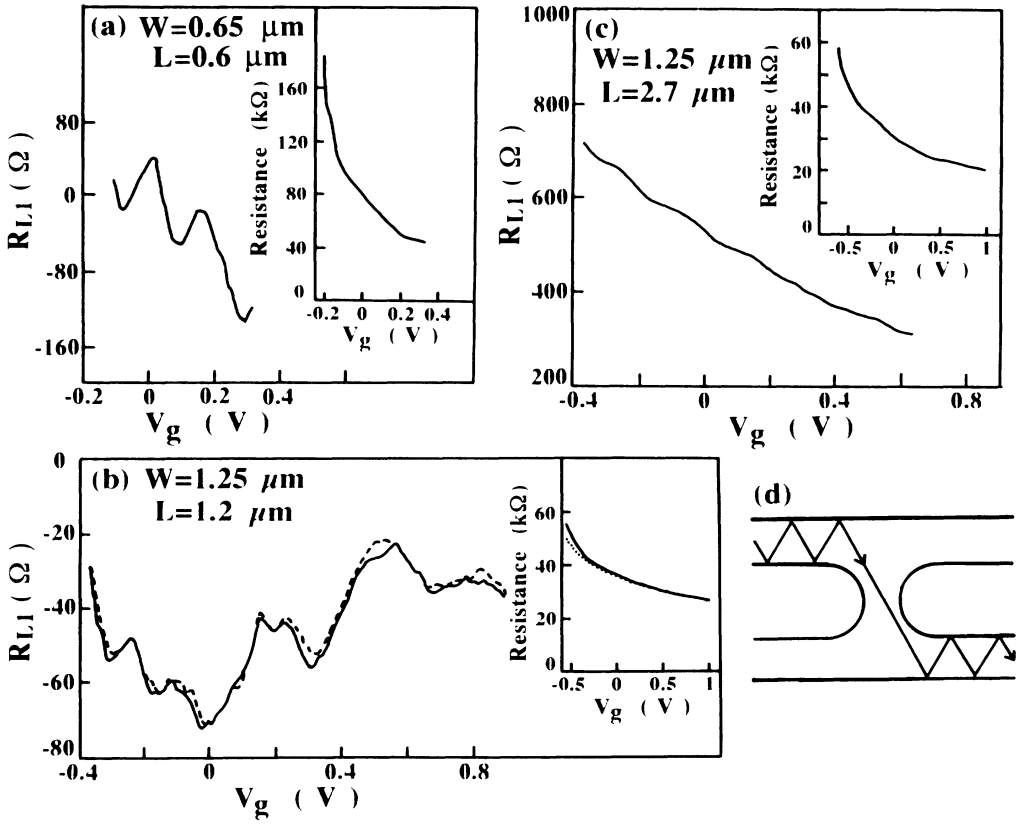


FIG. 4. $R_{L1}$ as a function of $V_g$ for several different structures measured at $B=0$ T. (a) $W=0.65$ μm and $L=0.6$ μm, (b) $W=1.25$ μm and $L=1.2$ μm , and (c) $W=1.25$ μm and $L=2.7$ μm. (a) was measured for a carrier density of $(2.2-2.6)\times10^{11}$ cm$^{-2}$ for $V_g=-0.1-0.25$ V, (b) was measured for the same conditions as for Fig. 3, and (c) was measured for a carrier density of $(1.5-1.7)\times10^{11}$ cm$^{-2}$. The broken curve in (b) indicates the reproducibility of the measurement. Each inset shows two-terminal resistance of the wire as a function of $V_g$. For structure (b), two-terminal resistance of another wire is also shown as a dotted line.

resistance of a wire $L_{\rm eff}\approx2.7$ μm-$2W_{\rm dep1}=1.9$ μm long and $W_{\rm eff}=2.5$ μm-$2W_{\rm dep2}$ wide [this value changes from 1.3 μm ($V_g=-0.4$ V) to 1.6 μm ($V_g=0.6$ V)]. This diffusive resistance decreases as the wire width increases with $V_g$. This is actually observed in Fig. 4(c) and this makes a striking contrast with the ballistic case [Fig. 4(b)], where the average value of $R_{L1}$ is negative and almost constant as a function of $V_g$. However, some sideways ballistic components remain even in the $L=2.7$-μm sample and weak oscillatory structures are still observable in Fig. 4(c).

## III. SUMMARY

We have studied the four-terminal (transfer) resistance ($R_{L1}$) of a system where two parallel IPG wires are coupled by a ballistic window. As this resistance essentially becomes almost zero for a wide range of magnetic-field and IPG voltages, it is sensitive to a small modulation in the electron flow in the ballistic window. In particular, the modulation of sideways ballistic components by subband depopulation is clearly observed in $R_{L1}$ at 1.5 K when the effective wire width is modulated using an in-plane-gated system. Magneto-depopulation of the subbands in each wire is also observed down to a low magnetic field in this system. In addition, the ballistic structure with both straight and rounded boundaries may result in a peculiar negative $R_{L1}$ in an intermediate-magnetic-field region.

## ACKNOWLEDGMENTS

We would like to thank A. Fischer and M. Hauser for their expert help with the MBE growth. Part of this work was sponsored by the Bundesministerium für Forshcung und Technologie of the Federal Republic of Germany.

*Present address: NTT Basic Research Laboratories, Musashino-Shi, Tokyo 180, Japan.
†Present address: Technische Hochschule Darmstad, Karolinenplatz 5, D-6100 Dalmstadt, Germany.

[1]B. J. van Wees *et al.*, Phys. Rev. Lett. **60**, 848 (1988); D. A. Wharam *et al.*, J. Phys. C **21**, L209 (1988).
[2]C. W. J. Beenakker and H. van Houten, in *Solid State Physics,* edited by H. Ehrenreich and D. Turnbull (Academic, Lon-

don, 1991), Vol. 44.

[3]B. J. van Wees *et al.*, Phys. Rev. Lett. **62**, 2523 (1989); C. G. Smith *et al.*, Surf. Sci. **228**, 387 (1990); Y. Hirayama and T. Saku, Solid State Commun. **73**, 113 (1990).

[4]S. E. Ulloa *et al.*, Phys. Rev. B **41**, 12 350 (1990); L. P. Kouwenhoven *et al.*, Phys. Rev. Lett. **65**, 361 (1990).

[5]C. G. Smith *et al.*, J. Phys. Condens. Matter **1**, 6763 (1989); Y. Hirayama and T. Saku, Phys. Rev. B **42**, 11 408 (1990).

[6]K. Ensslin and P. M. Petroff, Phys. Rev. B **41**, 12 307 (1990); D. Weiss *et al.*, Phys. Rev. Lett. **66**, 2790 (1991); A. Lorke *et al.*, Phys. Rev. B **44**, 3447 (1991).

[7]C. J. B. Ford *et al.*, Phys. Rev. B **43**, 7339 (1991); R. Behringer *et al.* Phys. Rev. Lett. **66**, 930 (1991).

[8]C. G. Smith *et al.*, J. Phys. Condens. Matter **1**, 9035 (1989).

[9]N. Tsukada *et al.* Appl. Phys. Lett. **56**, 2527 (1990); C. C. Eugster and J. A. del Alamo, Phys. Rev. Lett. **67**, 3586 (1992).

[10]Y. Takagaki *et al.*, Solid State Commun. **69**, 811 (1989); M. L. Roukes *et al.*, in *Electronic Properties of Multilayers and Low-Dimensional Semiconductor Structures,* edited by J. M. Chamberlain *et al.* (Plenum, London, 1990).

[11]Y. Hirayama *et al.*, Phys. Rev. B **39**, 5535 (1989); S. Nakata *et al.*, J. Appl. Phys. **69**, 3633 (1991).

[12]A. D. Wieck and K. Ploog, Appl. Phys. Lett. **56**, 928 (1990); T. Bever, *et al.*, Phys. Rev. B **44**, 3424 (1991); *ibid.* **44**, 6507 (1991).

[13]Transport characteristics of IPG wire structures fabricated by focused Ga-ion-beam scanning and subsequent annealing are planned to be discussed elsewhere by Y. Hirayama *et al.* (unpublished).

[14]Although it is difficult to get complete twofold symmetry in a real system, we select structures where the two-terminal resistances of parallel wires $[(V_1\text{-}V_2)/I_{1\text{-}2}$ and $(V_3\text{-}V_4)/I_{3\text{-}4}]$ agree within an error of less than 5% for the measured $V_g$ range.

[15]M. Büttiker, in *Nanostructure Systems,* edited by M. A. Reed (Academic, New York, 1990).

[16]Y. Takagaki *et al.*, Solid State Commun. **71**, 809 (1989); G. Timp *et al.*, in *Nanostructure Physics and Fabrication,* edited by M. A. Reed and W. P. Kirk (Academic, New York, 1990); C. W. J. Beenakker and H. van Houten, Phys. Rev. Lett. **63**, 1857 (1989); Y. Hirayma *et al.*, Appl. Phys. Lett. **58**, 2672 (1991).

[17]C. W. J. Beenakker *et al.*, Superlatt. Microstruct. **5**, 127 (1989); see also Ref. 2.

[18]K.-F. Berggren *et al.* Phys. Rev. Lett. **57**, 1769 (1986); Phys. Rev. B **37**, 10 118 (1988).

[19]Y. Avishai and Y. B. Band, Phys. Rev. Lett. **62**, 2527 (1989); G. Kirsczenow, Solid State Commun. **71**, 469 (1989); T. Kakuta *et al.*, Phys. Rev. B **43**, 14 321 (1991).

[20]A. G. Aronov and Yu. V. Sharvin, Rev. Mod. Phys. **59**, 755 (1987); S. Washburn, IBM J. Res. Dev. **32**, 335 (1988); R. A. Webb *et al.*, in *Physics and Technology of Submicron Structures,* edited by H. Heinrich *et al.* (Springer-Verlag, Heidelberg, 1988).

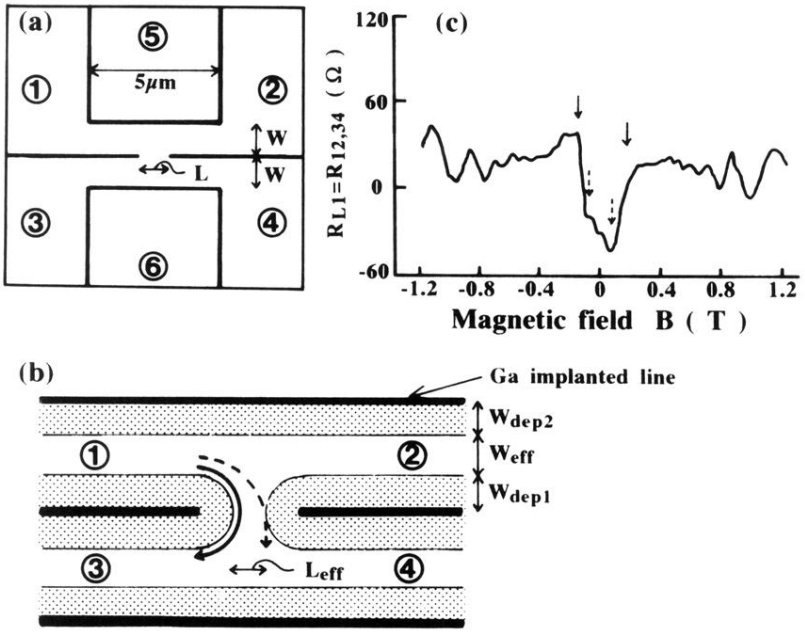


FIG. 1. (a) Schematic diagram of two parallel IPG wires coupled by a ballistic window. The focused Ga ion beam was scanned along the solid lines. (b) Magnified diagram around the window region. Dotted area represents the depletion region spreading. (c) Typical $R_{L1}=R_{12,34}$ vs magnetic-field characteristics of the structure with $W=1.25$ $\mu$m, $L=1.2$ $\mu$m, and $V_g=0$ V measured in a low magnetic field. The 2D carrier density is $1.8\times10^{11}$ cm$^{-2}$. Solid arrows indicate the magnetic field ($B=B_{c1}$) where the negative peak disappears and broken arrows indicate the magnetic field ($B=B_{c2}$) where a second peak or a kink appears in the negative peak.

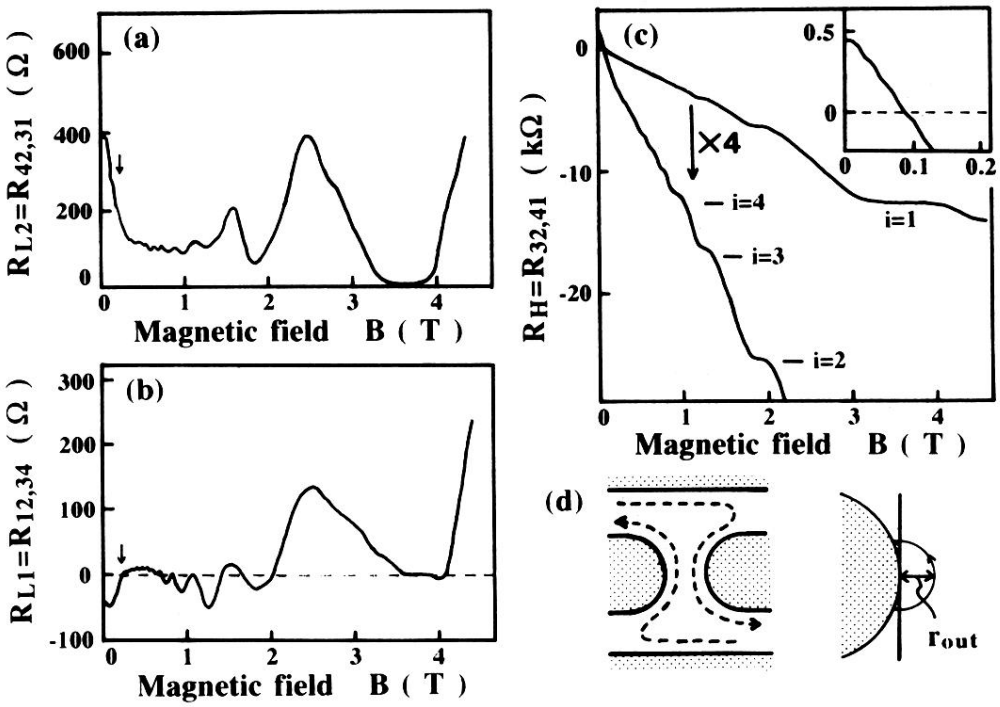


FIG. 2. (a) $R_{L2}=R_{42,31}$, (b) $R_{L1}=R_{12,34}$, and (c) $R_H=R_{32,41}$ obtained for the sample of Fig. 1 at $T=1.5$ K. The carrier density is $2\times10^{11}$ cm$^{-2}$ and $V_g=0$ V. Solid arrows indicate the approximate position of $B_{c1}$. The inset of (c) shows a magnification near $B=0$ T with the same axis labeling as the main figure. (d) A possible trajectory for the combination of straight and rounded boundaries (left) and the change in the area enclosed by a trajectory for straight and rounded boundaries with the same $r_{out}$ (right).